Development 135, 1713-1723 (2008) doi:10.1242/dev.015149

The mutation *ROR2*^{W749X}, linked to human BDB, is a recessive mutation in the mouse, causing brachydactyly, mediating patterning of joints and modeling recessive Robinow syndrome

Regina Raz[1], Sigmar Stricker[2], Elizabetta Gazzerro[3,4], Julie L. Clor[1], Florian Witte[2], Harakiran Nistala[1], Stefanie Zabski[1], Renata C. Pereira[3], Lisa Stadmeyer[3], Xiangmin Wang[1], Lori Gowen[1], Mark W. Sleeman[1], George D. Yancopoulos[1], Ernesto Canalis[3,4], Stefan Mundlos[2], David M. Valenzuela[1] and Aris N. Economides[1,*]

Mutations in *ROR2* result in a spectrum of genetic disorders in humans that are classified, depending on the nature of the mutation and the clinical phenotype, as either autosomal dominant brachydactyly type B (BDB, MIM 113000) or recessive Robinow syndrome (RRS, MIM 268310). In an attempt to model BDB in mice, the mutation W749X was engineered into the mouse *Ror2* gene. In contrast to the human situation, mice heterozygous for *Ror2*^{W749FLAG} are normal and do not develop brachydactyly, whereas homozygous mice exhibit features resembling RRS. Furthermore, both *Ror2*$^{W749FLAG/W749FLAG}$ and a previously engineered mutant, *Ror2*$^{TMlacZ/TMlacZ}$, lack the P2/P3 joint. Absence of *Gdf5* expression at the corresponding interzone suggests that the defect is in specification of the joint. As this phenotype is absent in mice lacking the entire *Ror2* gene, it appears that specification of the P2/P3 joint is affected by ROR2 activity. Finally, *Ror2*$^{W749FLAG/W749FLAG}$ mice survive to adulthood and exhibit phenotypes (altered body composition, reduced male fertility) not observed in *Ror2* knockout mice, presumably due to the perinatal lethality of the latter. Therefore, *Ror2*$^{W749FLAG/W749FLAG}$ mice represent a postnatal model for RRS, provide insight into the mechanism of joint specification, and uncover novel roles of *Ror2* in the mouse.

KEY WORDS: ROR2 receptor, Brachydactyly B, Phalanx formation, Knock-in mouse

INTRODUCTION

Recessive Robinow syndrome (RRS, MIM 268310) and autosomal dominant brachydactyly type B (BDB, MIM 113000) are two distinct syndromes caused by mutations in the *ROR2* gene (Afzal and Jeffery, 2003). RRS is characterized by moderately short stature, hemivertebrae, mesomelic limb shortening, brachydactyly, abnormal facial features and genital hypoplasia (Patton and Afzal, 2002). By contrast, BDB is characterized by hypoplasia of the distal and middle phalanges with variable degrees of distal and proximal symphalangism, often accompanied by nail dysplasia (Schwabe et al., 2000).

ROR2 belongs to a small family of receptor tyrosine kinases containing frizzled domains (Forrester, 2002). The extracellular region is characterized by the presence of immunoglobulin (Ig), frizzled-like cystein-rich (Frz or CRD) and kringle (Kr) domains, all postulated to mediate protein-protein interactions. The intracellular region contains a tyrosine kinase (TK) domain, and a conserved domain consisting of two regions rich in serine and threonine (ST1, ST2) flanking a region rich in proline (PR). Based on the homology of its Frz domain to a corresponding domain in the Wnt receptors, the Frizzleds, ROR2 was proposed, and then shown, to act as a receptor for Wnts (Masiakowski and Yancopoulos, 1998; Saldanha et al., 1998; Hikasa et al., 2002; Billiard et al., 2005; Oishi et al., 2003; Mikels and Nusse, 2006).

[1]Regeneron Pharmaceuticals, Inc., Tarrytown, NY, USA. [2]Max-Planck Institute for Molecular Genetics Berlin, and Institute for Medical Genetics, University Medicine Berlin, Charité, Berlin, Germany. [3]Saint Francis Hospital and Medical Center, Hartford, CT, USA. [4]The University of Connecticut School of Medicine, Farmington, CT, USA.

*Author for correspondence (e-mail: aris.economides@regeneron.com)

Accepted 26 February 2008

The genetic lesions found in RRS patients consist of homozygous missense, nonsense and frameshift mutations affecting the Frz, Kr and TK domains of ROR2. They are predicted to eliminate or severely reduce receptor function and are thus thought to be loss-of-function mutations (Forrester, 2002). Consistent with this hypothesis, knockouts of *Ror2* in the mouse cause a developmental phenotype that displays some of the features of RRS, such as short limbs and brachydactyly, as well as genital, cardiac and craniofacial defects (DeChiara et al., 2000; Takeuchi et al., 2000). By contrast, mutations in *ROR2* causing autosomal dominant BDB cluster within two segments immediately upstream and downstream of the TK-encoding region, and are all predicted to result in truncations of the intracellular domain (Schwabe et al., 2000). Because neither heterozygous carriers of RRS nor individuals with chromosomal deletions encompassing *ROR2* exhibit digit defects (Oldridge et al., 1999), it appears unlikely that the BDB mutations have a loss-of-function effect and it is instead thought that they confer novel gene functions (Forrester, 2002).

In this study, we use a knock-in approach in mice to assess the effect of *ROR2*^{W749X}, one of the mutations identified in individuals with severe forms of BDB. Unlike *Ror2* knockout mice (Takeuchi et al., 2000; DeChiara et al., 2000), *Ror2*$^{W749FLAG/W749FLAG}$ animals are viable, allowing the study of the effect of this ROR2 truncation postnatally. This animal model exhibits many of the features of RRS, and uncovers novel phenotypes in fertility and body composition. In addition, a differential phenotypic trait, restricted to the digits, was observed between mutants missing the entire *Ror2* coding region versus the *Ror2*$^{TMlacZ/TMlacZ}$ and *Ror2*$^{W749FLAG/W749FLAG}$ lines. Our observations point to a direct role of ROR2 cytoplasmic mutations in the modulation of joint specification.

MATERIALS AND METHODS

Generation of knock-in mice, genotyping and RT-PCR assays

Ror2^{W749FLAG} mice were generated using VelociGene technology (Valenzuela et al., 2003). Briefly, a bacterial artificial chromosome-based targeting vector (BACVEC) was used to replace the sequence coding for domain G750-D930 of mouse ROR2 with the FLAG epitope, followed by a neomycin resistance cassette. ESC transfection, chimera production and genotyping of offspring were as described (Valenzuela et al., 2003). Embryos were genotyped by allele-specific PCR on yolk sac DNA, using the primers: 5′-CTTCCCACAGCCTCAGTTCATC-3′, 5′-TCACCTGGAGCGTGTCATTGTC-3′, 5′-GACTACAAAGACGATGACGACAAGC-3′ and 5′-TGGATGTGGAATGTGTGCGAG-3′. RNA was isolated with the RNeasy kit (Qiagen, Valencia, CA, USA) from 15.5 days post-coitum (dpc) embryos preserved in RNAlater (Ambion, Austin, TX, USA). First-strand cDNA and PCR amplification were performed as described (Marie et al., 1998), using the primers: 5′-ATTCACTGCTGCCCATCCGC-3′, 5′-GATGAACTGAGGCTGTGGGAAGG-3′ and 5′-GCTTGTCGTCATCGTCTTTGTAGTC-3′.

Immunoprecipitation and western blotting

Immunoprecipitation followed by protein G-Sepharose (Amersham Biosciences, Piscataway, NJ, USA) precipitation was performed on tissue lysates (1% Brij 96 buffer) with either an anti-FLAG antibody (M2, Sigma-Aldrich, St Louis, MI, USA) or a rabbit anti-ROR2 antibody against the 80 carboxy-terminal amino acids. Immunoprecipitates were separated by SDS/PAGE, immunoblotted with antibodies to ROR2, FLAG or phosphotyrosine (4G10, Millipore, Billerica, MA, USA), and visualized by chemiluminescence (SuperSignal West Pico, Pierce, Rockford, IL, USA).

Expression constructs, transient transfection and confocal imaging

ROR2 constructs were generated with the QuikChange mutagenesis kit (Stratagene, La Jolla, CA, USA), cloned into pcDNA3.1 (Invitrogen, Carlsbad, CA, USA) and transfected into Cos1 cells with ExGene500 (Fermentas, Burlington, Canada). Detection was with an anti-human ROR2 antibody (R&D Systems, Minneapolis, MN, USA) followed with Alexa Fluor 568 anti-human IgG (Molecular Probes, Eugene, OR, USA). Counterstaining was with 4′,6-diamidino-2-phenylindole (DAPI). Images were generated on a Zeiss Axiovert 2000 microscope with ApoTome optics (Zeiss, Jena, Germany).

Body composition analysis

Body composition and length were measured on anesthetized mice by dual-emission X-ray absorptiometry (pDEXA Sabre X-Ray Bone Densitometer and software, Norland Medical Systems, Ft. Atkinson, WI, USA). Quality assurance measurements were performed prior to each use. Measurements were an average of two consecutive scans per animal.

Fertility assessment tests

Ror2$^{W749FLAG/W749FLAG}$ and *Ror2*$^{+/W749FLAG}$ littermate males (n=6) were mated with CD-1 virgin females not selected for oestrus. For each trial mating, one female was brought to the male's cage and separated the following day. Testing continued until each male had been mated with 10 females. The percentages of females presented to each male that exhibited a vaginal plug and that became pregnant were calculated as indexes of plugging rate and pregnancy rate.

Sperm collection, sperm analysis and in vitro fertilization (IVF) assays

The content of the vas deferens and cauda epididymis was released into HTF-0.4% BSA (human tubal fluid, Conception Technologies, San Diego, CA, USA) and analyzed using the Hamilton Thorne Biosciences IVOS System with Animal Motility Software (Beverly, MA, USA). For IVF assays, cumulus-oocyte-complexes from superovulated B6C3F1/Crl females were incubated with sperm in 500-μl drops of HTF-BSA at 37°C. Fertilized embryos were transferred 4 to 6 hours later to 75-μl drops of KSOM (Specialty Media, Phillipsburg, NJ, USA) for overnight culture. Two-cell embryos were then evaluated, transferred to fresh KSOM and cultured for 72 hours to the expanded-blastocyst stage. Assays were performed on 3-month-old *Ror2*$^{W749FLAG/W749FLAG}$, *Ror2*$^{+/W749FLAG}$ and control littermates (n=3).

Skeletal analysis and histology

Cleared skeletal preparations were prepared as described (Lufkin et al., 1992; Jegalian and De Robertis, 1992). Cell proliferation analysis in vivo was carried out by injection of 5-bromo-deoxyuridine (BrdU, Calbiochem, San Diego, CA, USA) at 50 mg/kg 2 hours before euthanasia. For E18.5 and P5 analysis, limbs were formalin fixed and decalcified (Decal Stat High Speed, Decal Corporation, Tallman, NY, USA). Humeri and femurs were then dissected and embedded in Tissue-Tek OCT (Miles, Elkhart, IN, USA). Staining of frozen sections was done with the Dako EnVision+ System and BrdU antibody (Dako, Glostrup, Denmark). Quantitation of BrdU-positive cells was performed with NIH Image (NIH, Bethesda, MD, USA) on six sections from two mice. For E12.5 analysis, limb sections were stained with the BrdU Labeling and Detection Kit II (Roche Applied Science, Indianapolis, IN, USA) and counterstained with DAPI to visualize nuclei. Proliferation rates were calculated from four sections, as the number of BrdU-positive nuclei relative to the total number of nuclei. For prepubertal testes histology, 10-μm frozen sections were stained with Hematoxylin. All other histology was performed on paraffin-embedded tissues by Charles River Laboratories (Wilmington, MA, USA).

In situ hybridization

In situ hybridization was performed on 7-μm paraffin sections of limbs, using digoxigenin-labeled riboprobes prepared as described (Stricker et al., 2002). Whole-mount hybridizaton was performed as described (Albrecht et al., 2002). Photography was with a binocular microscope and camera (Leica, Bensheim, Germany). The riboprobes used were: *Sox9* (Healy et al., 1996), *Hoxd11*, *Hoxd12*, *Hoxd13*, *Gdf5*, *Fgf8* and *Shh* (Albrecht et al., 2002).

X-ray and bone histomorphometric analysis

Radiography was performed post-mortem at 30 kV for 20 seconds (MX 20, Faxitron X-ray, Wheeling, IL, USA). For histomorphometry, mice were injected with 20 mg/kg calcein and 50 mg/kg demeclocycline at an interval of 2, 5 or 7 days (for 3-, 8- and 24-week old mice, respectively), and sacrificed 2 days after the demeclocycline injection. Dissected femurs were fixed in 70% ethanol, dehydrated and embedded undecalcified in methyl methacrylate. Longitudinal 5-μm sections were cut on a Microm microtome (Richard-Allan Scientific, Kalamazoo, MI, USA) and stained with 0.1% Toluidine Blue, pH 6.4. Static parameters of bone turnover were measured in a defined area between 725 μm and 1270 μm from the growth plate, using OsteoMeasure (Osteometrics, Atlanta, GA, USA). Dynamic histomorphometric parameters were measured as described (Gazzerro et al., 2005). Terminology and units are as recommended by the ASBMR Histomorphometry Nomenclature Committee (Parfitt et al., 1987).

RESULTS

Engineering mice carrying a targeted truncation of ROR2 at W749

ROR2^{W749X}, resulting from a 2246G→A transition mapping downstream of the tyrosine kinase domain (Fig. 1A), is one of several heterozygous mutations found in families affected with classical BDB disorder (Oldridge et al., 2000). To investigate the basis for the two different syndromes associated with *Ror2* mutations, we generated knock-in mice expressing ROR2 truncated at W749 and tagged at the carboxyl terminus with the FLAG epitope (*Ror2*^{W749FLAG}; Fig. 1B). Experimental cohorts were genotyped by PCR (Fig. 1C). Transcription of the truncated ROR2-W749FLAG transcript was verified by RT-PCR (Fig. 1D). Expression and tyrosine phosphorylation of the truncated receptor were confirmed by immunoprecipitation from uterus lysates (Fig. 1E). Like ROR2, ROR2-R747FLAG, a mutein very similar to ROR2-W749FLAG, localizes to the membrane (Fig. 1F,G; identical results have been obtained with ROR2-W749FLAG, not shown).

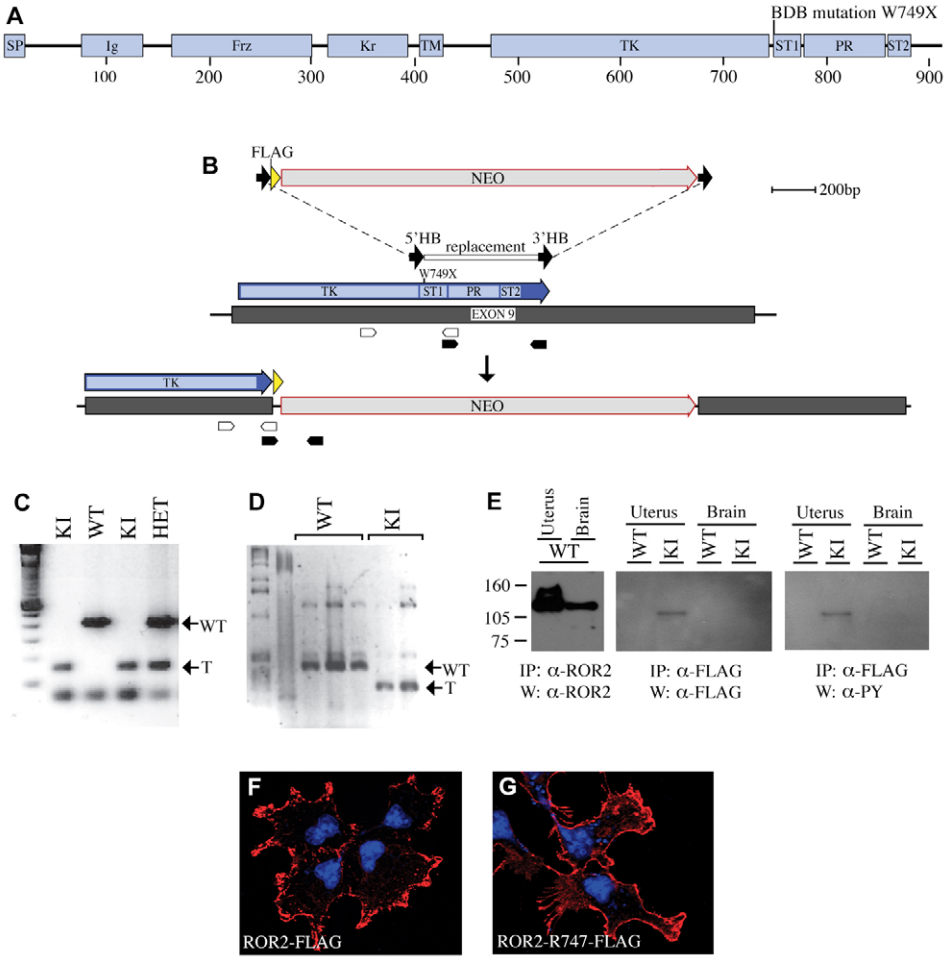

Fig. 1. Targeted truncation of ROR2 at W749. (**A**) Structure of the ROR2 receptor showing the immunoglobulin-like (Ig), frizzled-like (Frz), kringle (Kr), transmembrane (TM), tyrosine-kinase (TK), serine/threonine-rich (ST1, ST2) and proline-rich (PR) domains, and the site of the BDB mutation (black line). SP, signal peptide. (**B**) Targeting strategy in the region spanning the last exon of *Ror2*, encoding the TK and ST1/PR/ST2 domains. The targeting vector carries a replacement of the region encoding W749-D930 with a FLAG-encoding sequence fused in frame, followed by a selectable marker (NEO, neomycin resistance gene). Target sites for primers are indicated by white (cDNA genotyping) and black (genomic genotyping) arrowheads. (**C**) PCR analysis of yolk sac DNA from wild-type and mutant embryos showing the products from the wild type (WT, 419 bp) and targeted (T, 174 bp) alleles. (**D**) RT-PCR analysis confirming the loss of wild type *Ror2* mRNA (455 bp product, WT) in *Ror2*$^{W749FLAG/W749FLAG}$ E15.5 embryos (KI), and the presence of mRNA for the truncated ROR2 (321 bp product, T). (**E**) Immunoblot analysis of ROR2 receptor from wild-type (WT) and *Ror2*$^{W749FLAG/W749FLAG}$ (KI) tissues. Antibodies used for immunoprecipitation (IP) and western (W), and sizes (kDa) and migration of molecular standards, are indicated. (**F**,**G**) Confocal microscopy of full-length and truncated ROR2 receptors overexpressed in Cos1 cells.

Altered body mass and skeletal defects in *Ror2*$^{W749FLAG/W749FLAG}$ mutant mice

Homozygous mutant mice were born at the expected Mendelian ratio and were viable. Whereas *Ror2*^{W749X} is transmitted as a dominant mutation in BDB patients, heterozygous *Ror2*$^{W749FLAG/+}$ mice were normal and did not display brachydactyly. Homozygous mutant mice appeared smaller (Fig. 2B,D) and exhibited a significant decrease in body weight, apparent before weaning (Fig. 2G). Body composition analysis revealed that *Ror2*$^{W749FLAG/W749FLAG}$ mice had significantly decreased fat mass and increased lean mass relative to their body weight (Fig. 2I). To determine whether the reduced body mass of *Ror2*$^{W749FLAG/W749FLAG}$ mice was accompanied by alterations in metabolic rate, we measured food intake, activity, energy expenditure, oxygen consumption and carbon dioxide production. No significant differences between mutant and wild-type littermates were found in any metabolic parameter, or in glucose or insulin tolerance tests (not shown).

Homozygous *Ror2*$^{W749FLAG/W749FLAG}$ had multiple craniofacial defects. They presented with a shorter snout and epiphora, which deteriorated with age and was often associated with entropion (Fig. 3A). Adult homozygous mutants showed significant shortening and broadening of the nasal bones (Fig. 3B,E,F), as well as significant shortening of the mandible, due to reduced length in the anterior region, from the infradentale to menton landmarks (Fig. 3D,H). The intra-orbital width was significantly increased in mutant mice (Fig. 3B,G). In the postcranial skeleton, all homozygous mice exhibited a reduced longitudinal axis, brachydactyly in the fore and hind paws (detailed analysis below) and, in 5% of the cases, a bifid digit I in the right hind feet. In addition, 25% of the homozygous mutants had one or more tail kinks (Fig. 2B). Body length, but not width, was significantly decreased in adult *Ror2*$^{W749FLAG/W749FLAG}$ mice (9.5±0.18 cm versus 10.4±0.25 cm, P=0.005). The shortening of the longitudinal axis resulted from hypoplastic vertebral bodies, rather than from a reduced number of vertebrae (Fig. 2D). Tail kinks were caused by hemivertebrae (Fig. 2E, arrows). In addition, fusions of caudal vertebrae were observed in 5% of the mutants (Fig. 2E, arrowhead). Stylopod and zeugopod bones were shorter by 12%-19% in *Ror2*$^{W749FLAG/W749FLAG}$ mice of weaning age; however, the differences between mutant and controls became less marked as the animal aged (see Table S1 in the supplementary material). In the autopod, most phalanges and metacarpals remained significantly shorter than in controls (up to 27%, P<0.01; see Table S2 in the supplementary material).

Ror2^{W749FLAG} mutation does not affect bone remodeling in adult mice

ROR2 has been reported to have signaling activity in osteoblastic cells and to promote osteoblastic activity in vitro (Billiard et al., 2005; Liu et al., 2006), whereas *Ror2* knockout embryos exhibit delayed ossification of endochondral bones (DeChiara et al., 2000). We were therefore interested in determining whether ROR2-W749FLAG has an effect in the regulation of bone formation. No abnormalities could be detected in bone histomorphometric

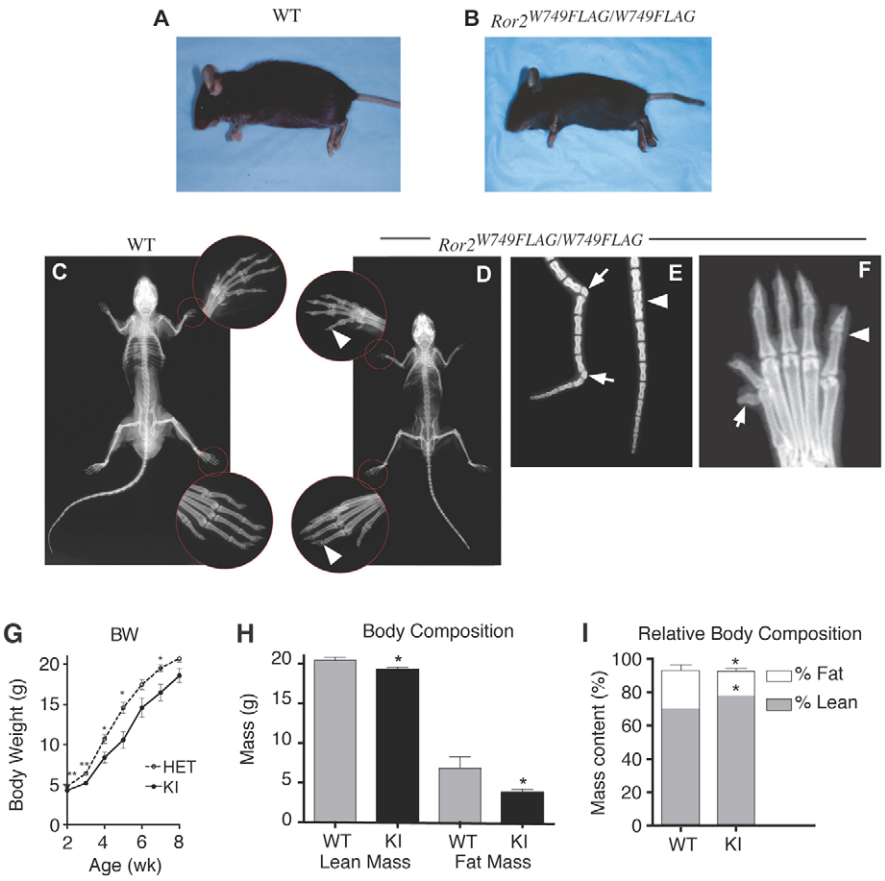

Fig. 2. Reduced body mass, altered body composition and skeletal defects of *Ror2*$^{W749FLAG/W749FLAG}$ mutants.
(**A**,**B**) Comparison of 5-month-old control (A) and *Ror2*$^{W749FLAG/W749FLAG}$ littermate (B) mice; the mutants display a smaller body and a shorter, kinked tail. (**C-F**) Radiographic analysis of skeletons from wild-type (C) and *Ror2*$^{W749FLAG/W749FLAG}$ (D-F) adult mice. *Ror2*$^{W749FLAG/W749FLAG}$ animals display reduced length of the axial skeleton due to shorter vertebrae (D) and have a missing phalange in digits II-IV (inset, arrowheads). (E) Distal tail radiography from two mutant mice showing fused vertebrae (arrowhead) and hemivertebrae with misaligned articular surfaces, causing tail kinks (arrows). (F) Right hindlimb radiography from a *Ror2*$^{W749FLAG/W749FLAG}$ mouse with preaxial polydactyly (arrow). Note a missing phalanx in all the other digits (arrowhead). (**G**) Weight curves of heterozygous (HET) and homozygous (KI) *Ror2*^{W749FLAG} male mice from a single litter, n=3-4. (**H**) Measurements of lean and fat mass in *Ror2*$^{W749FLAG/W749FLAG}$ mice (KI) and litter-matched wild-type controls (WT). (**I**) Percentage fat mass (white stacked bar) and lean mass (dotted bar) in *Ror2*$^{W749FLAG/W749FLAG}$ mice (KI) and controls (WT). Eight *Ror2*$^{W749FLAG/W749FLAG}$ and five wild-type littermate male mice were evaluated at 21 weeks of age (H,I). Values are means±s.e.m. Significantly different from controls: $^{**}P<0.01$; $^{*}P<0.05$.

parameters in femurs from 8- to 24-week-old *Ror2*$^{W749FLAG/W749FLAG}$ mice (Fig. 4C), suggesting that *Ror2* does not exert a significant action on the regulation of adult bone remodeling. In actively growing femurs from 3-week-old *Ror2*$^{W749FLAG/W749FLAG}$ mice, a 52% reduction in trabecular bone volume was observed associated with a 57% decrease in the number of trabeculae. There was no change in the number of osteoblasts per perimeter (not shown), or in the osteoblast surface/bone surface. A lower value of the calculated number of osteoblasts/area was due to lower bone area. Dynamic histomorphometry indicated that the mineral apposition rate was lower in the mutants than in controls, suggesting a reduced osteoblastic function. However, the mineralizing surface per bone surface was higher in the mutant femurs, resulting in an elevation of the calculated bone formation rate. In summary, the low bone volume and the high bone formation rate observed in 3-week-old animals are accompanied by normal osteoblast number; they resolve later in life, and may therefore represent a delay in the process of endochondral ossification in mutant animals rather than a defect in osteoblast differentiation and function.

Ror2$^{W749FLAG/W749FLAG}$ male mice display reduced fertility

In trial matings with CD-1 mice, female *Ror2*$^{W749FLAG/W749FLAG}$ proved fertile, whereas *Ror2*$^{W749FLAG/W749FLAG}$ males showed decreased fertility, reflected by a 4% pregnancy rate versus 15% for heterozygous controls (Fig. 5A). *Ror2*$^{W749FLAG/W749FLAG}$ males had a lower combined testicular weight (118±9 mg versus 165±8 mg, P=0.002, 2-month-old animals), which was also significant after correction for their reduced body weight (Fig. 5B). Histologically, early puberty *Ror2*$^{W749FLAG/W749FLAG}$ testes (16 days) showed a decreased density of seminiferous tubules (Fig. 5D). In addition, most tubules had a reduced diameter and

Table 1. *Ror2*$^{W749FLAG/W749FLAG}$ spermatozoa are functional

Animal*	Plugged superovulated female	Spermatozoa motility (%)	Spermatozoa concentration (million/ml)	Progressive spermatozoa (%)	IVF rate† (%)	Number of blastocysts/2-cell embryos (%)
B6D2F1	Yes	71	38.1	56	66/83 (79.5%)	64/66 (96.9%)
WT-1	No	71	29.6	49	23/87 (26.4%)	23/23 (100.0%)
WT-2	Yes	66	21.0	45	23/83 (27.7%)	22/23 (95.6%)
WT-3	Yes	73	55.5	54	55/109 (50.4%)	52/55 (94.5%)
KI-1	No	63	22.1	44	63/96 (65.6%)	62/63 (98.4%)
KI-2	No	74	25.1	58	61/106 (57.5%)	59/61 (96.7%)
KI-3	No	63	22.3	43	55/81 (67.9%)	53/55 (96.4%)

*Three-month-old males, homozygous mutant (KI) and wild-type (WT) littermates.
†Two-cell embryos/fertilized oocytes.

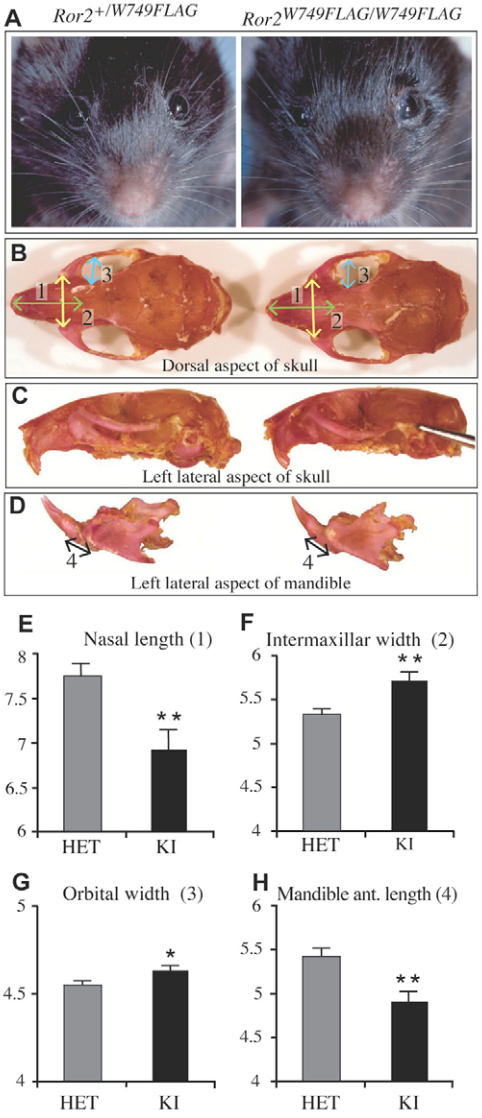

Fig. 3. The craniofacial defects in *Ror2*$^{W749FLAG/W749FLAG}$ mutants are due to changes in the nasal bones and orbital width. (**A**) Facial phenotype of *Ror2*$^{W749FLAG/W749FLAG}$ mice (right), showing shorter snout, increased intercanthal distance and entropion eyes. (**B-D**) Comparison of crania from heterozygous control (left) and homozygous mutant (right) *Ror2*^{W749FLAG} mice (9-month-old males), viewed from dorsal (B) and lateral (C,D) aspects. The double arrows indicate the craniometric linear measurements that showed significant differences: (1) nasal length, (2) intermaxillar width, (3) intraorbital width and (4) mandible anterior length. (**E-H**) Average lengths and widths (mm) of craniometric parameters that were significantly different between *Ror2*$^{W749FLAG/W749FLAG}$ mice and control littermates. Values represent the mean±s.e.m. of triplicate measurements from five heterozygous (HET) and five homozygous (KI) mice. Significantly different from controls: ***P*<0.01; **P*<0.05.

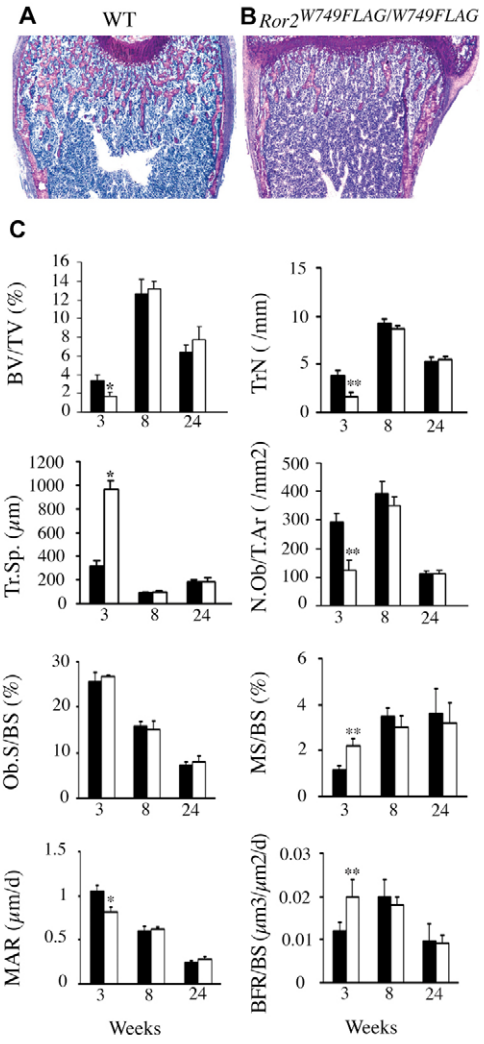

Fig. 4. Transient decrease in trabecular bone volume in *Ror2*$^{W749FLAG/W749FLAG}$ mutants. (**A**,**B**) Representative femur sections from a 3-week-old *Ror2*$^{W749FLAG/W749FLAG}$ mouse (B) and a wild-type littermate (A), stained with Toluidine Blue. (**C**) Static and dynamic histomorphometric parameters in *Ror2*$^{W749FLAG/W749FLAG}$ male mice (white bars) and control littermates (black bars) at 3, 8 and 24 weeks. Parameters analyzed were: bone volume/tissue volume (BV/TV, %); trabecular number (Tr.N, /mm); trabecular separation (Tr.Sp, μm); number of osteoblasts/tissue area (N.Ob/T.Ar, /mm^2); osteoblast surface/bone surface (Ob.S/BS, %); mineralizing surface/bone surface (MS/BS, %); mineral apposition rate (MAR, μm/day); bone formation rate/bone surface (BFR/BS, μm^3/μm^2/day). For static histomorphometry, sections were stained with Toluidine Blue. For dynamic histomorphometry, unstained sections were analyzed by fluorescence microscopy. Values are means±s.e.m. (*n*=6-11). Significantly different from controls: ***P*<0.01; **P*<0.05.

contained a single basal cell layer (Fig. 5F), as opposed to control testes, where all the tubules had a multilayered seminiferous epithelium. This abnormal histology partially resolved in adulthood, when degenerative tubules devoid of germ cells were seen only in focal areas of the testis (Fig. 5G). Numerous sperm were noted in the epididymis and ductus deferens, and accessory sex glands were normal. Consistent with the decreased testicular weight, the number of sperm cells collected from *Ror2*$^{W749FLAG/W749FLAG}$ testis was decreased (*P*=0.04; Table 1). However, mutant and control spermatozoa performed equally well in motility and IVF assays (Table 1). Therefore, the *Ror2*^{W749FLAG} mutation results in delayed germ cell differentiation

during puberty and decreased sperm production in the adult mouse, but does not affect overall sperm function or fertilizing ability.

Ror2$^{W749FLAG/W749FLAG}$ mice have defects in early chondrogenic condensation and distal joint specification

To analyze the progression of the skeletal phenotype, embryonic skeletal stains were prepared. At E18.5, no abnormalities were observed in the heterozygotes, whereas homozygous embryos displayed defects in the limbs and spine (Fig. 6N,Q,T). We observed delayed ossification of metacarpals, metatarsals and phalanges, and missing P2 (Fig. 6Q,T). Intervertebral discs were shortened, and 20% of the embryos presented one or two misshapen thoracic vertebrae with rib fusion of the associated ribs (Fig. 6N). These defects represent a subset of the abnormalities displayed by *Ror2* knockout embryos [described in detail elsewhere (DeChiara et al., 2000; Schwabe et al., 2004), and shown in Fig. 6L,O,R,U for comparison], and are milder. At E14.5, *Ror2*$^{W749FLAG/W749FLAG}$ embryos displayed hypoplastic skeletons, with a reduction in the size of all the anlagens, including the Meckel's and nasal cartilages (Fig. 6B). Vertebral deformities and tilting were apparent at this stage (Fig. 6E), but, with the exception of impaired segmentation of the digital rays (Fig. 6H), patterning was normal. These abnormalities are reminiscent of those exhibited by *Ror2*$^{TMlacZ/TMlacZ}$ E14 embryos (Fig. 6C,F,I), but are not as severe. Because the cartilaginous elements of *Ror2*$^{W749FLAG/W749FLAG}$ embryos displayed anatomical defects consistent with those observed in the skeletons of perinatal and adult mice, we conclude that the function mediated by the carboxy-terminal domain of ROR2 is required prior to E14.5, at the time of cartilaginous condensation.

Histological examination of *Ror2*$^{W749FLAG/W749FLAG}$ E13.5 embryos revealed a reduced number of cells in the chondrogenic condensations, whereas cell density did not appear to be affected (Fig. 7B,E,F). Cartilage matrix production by the chondrocytes was evaluated histologically using HAB (Hematoxylin, Alcian Blue) or HGF (Hematoxylin, Fast Green, Basic Fuschin), which stain for proteoglycans (blue) and collagen-associated proteoglycans (fuchsia), respectively (Ippolito et al., 1983; Tribioli and Lufkin, 1999). There were no differences in the pattern or intensity of the matrix stain in chondrocytic condensations at any stage between E13.5 and E15.5 (Fig. 7C-H).

Once the cartilage anlagens formed, their program of development proceeded normally in *Ror2*$^{W749FLAG/W749FLAG}$ mutants, except for a delay in the onset of developmental hallmarks, such as hypertrophy and vascularization (Fig. 7G,H), which translated into a slight reduction of bone length at birth (Fig. 7I,J). However, no change could be detected between mutants and controls in the proliferation rates of condensation or growth plate chondrocytes (Fig. 7K-N). These findings, together with the histological observations, indicate that the *Ror2*$^{W749FLAG/W749FLAG}$ skeletal phenotype is not caused by an altered proliferation or differentiation of chondrocytes, but rather by an impaired recruitment of mesenchymal cells into the chondrogenic condensation.

Ror2^{W749FLAG} interferes with specification of the distal digital interzone upstream of *Gdf5*

An intriguing aspect of the phenotypes associated with the *Ror2* allelic panel is that both *Ror2*$^{W749FLAG/W749FLAG}$ and *Ror2*$^{TMlacZ/TMlacZ}$ embryos, expressing truncated ROR2, lack phalanges P2. This stands in marked contrast to *Ror2*$^{-/-}$ embryos, where all the elements of the digit are formed (Schwabe et al., 2004) (Fig. 6U), indicating

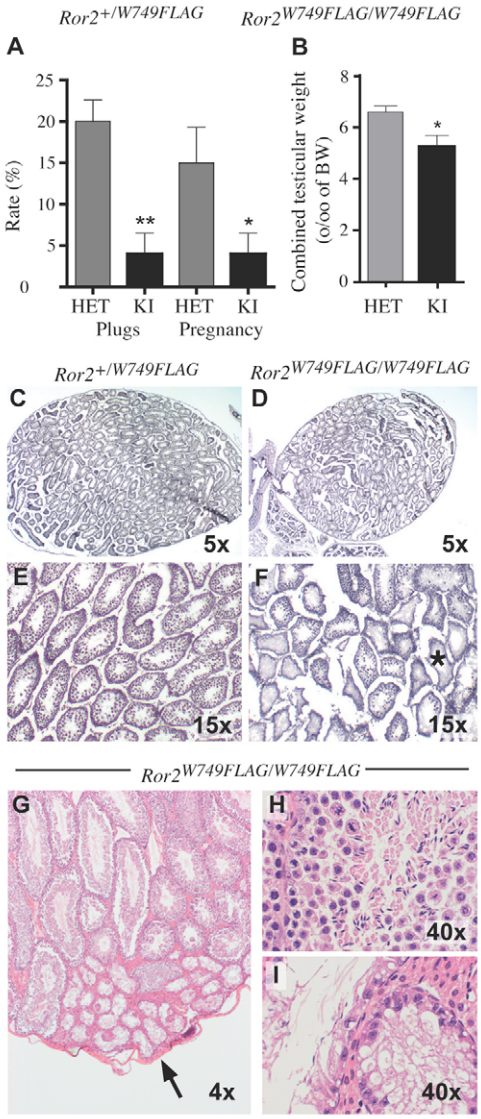

Fig. 5. Compromised fertility of *Ror2*$^{W749FLAG/W749FLAG}$ males. (**A**) Percentage of test females that became plugged or pregnant after controlled mating with *Ror2*$^{+/W749FLAG}$ (gray bars, HET) or *Ror2*$^{W749FLAG/W749FLAG}$ (black bars, KI) littermate mice. Values are mean±s.e.m. (n=60 matings, 10 matings per male). (**B**) Relative combined testicular weight, expressed as a per mille (‰) of body weight (BW), in *Ror2*$^{W749FLAG/W749FLAG}$ (black bars, KI) and control (gray bars, HET) littermates. Values are mean±s.e.m. (n=6, 2- to 3-month-old males). Significantly different from controls: $^{**}P<0.01$; $^{*}P<0.05$. (**C-F**) Histology of heterozygous (C,E) and homozygous (D,F) *Ror2*^{W749FLAG} testes from 16-day-old animals. The homozygous gonad exhibited decreased tubular density, with seminiferous tubules containing a single cell layer (asterisk). (**G-I**) Histology of a *Ror2*$^{W749FLAG/W749FLAG}$ testes (2-month-old) showing a focal area of tubular degeneration (G, arrow). (H) High magnification of a normal seminiferous tubule in the mutant testis. (I) High magnification of an abnormal seminiferous tubule, lined by clumps of Sertoli cells along the basal membrane and devoid of spermatogonia or spermatids.

that ROR2 function is dispensable for specification of the distal digit joint, yet truncated ROR2 receptors lacking either part or all of the cytoplasmic domain interfere, in homozygosis, with normal

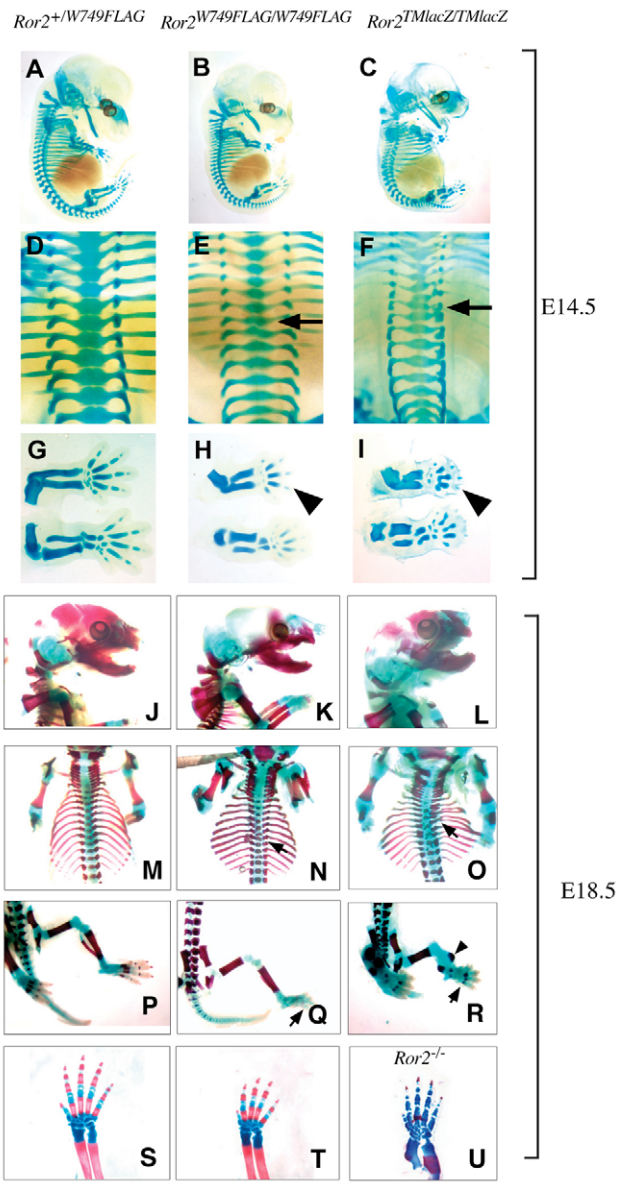

Fig. 6. The defects in skeletogenesis in *Ror2*$^{W749FLAG/W749FLAG}$ mutants stem from abnormalities in early chodrogenic condensation and specification of the distal digital joint. (**A-I**) Whole-mount cartilage staining of *Ror2*$^{W749FLAG/W749FLAG}$ (center) and heterozygous litter-matched E14.5 embryos (left), compared with *Ror2*$^{TMlacZ/TMlacZ}$ embryos (right). (A-C) Lateral view showing the reduction of all skeletal elements in *Ror2*$^{W749FLAG/W749FLAG}$ and *Ror2*$^{TMlacZ/TMlacZ}$ embryos. (D-F) Dorsal view of the thoracic spine. *Ror2*$^{W749FLAG/W749FLAG}$ and *Ror2*$^{TMlacZ/TMlacZ}$ vertebrae are hypoplastic and irregularly stacked (arrows). (G-I) Dissected forelimbs (top) and hindlimbs (bottom), showing reduced cartilage condensations in the homozygous mutant embryos. Note the absence of joint formation in the phalanx anlagens of the mutant forelimbs (arrowheads) and the greater reduction of condensation size in the *Ror2*$^{TMlacZ/TMlacZ}$ limbs. (J-T) Cleared skeletal preparations from control *Ror2*$^{+/W749FLAG}$ (left), *littermate Ror2*$^{W749FLAG/W749FLAG}$ (center) and *Ror2*$^{TMlacZ/TMlacZ}$ (right) E18.5 embryos. (**J-L**) Side view of skulls showing shortened nasal bones in the homozygous mutant embryos. (**M-O**) Dorsal view of ribcages showing smaller and tilted vertebrae in *Ror2*$^{W749FLAG/W749FLAG}$ and *Ror2*$^{TMlacZ/TMlacZ}$ embryos (N,O, arrows). Fused ribs were present with full penetrance in *Ror2*$^{TMlacZ/TMlacZ}$ embryos (O). (**P-R**) View of the hindlimb showing delayed ossification of metacarpals and phalanges in the homozygous mutant embryos (Q,R, arrows) and a severely misshapen *Ror2*$^{TMlacZ/TMlacZ}$ stylopod (arrowhead). (**S-U**) Comparison of control *Ror2*$^{+/W749FLAG}$ and *Ror2*$^{W749FLAG/W749FLAG}$ forepaws (S,T) with a *Ror2*$^{-/-}$ forepaw (U). Note the normal number of phalanges in the *Ror2*$^{-/-}$ digits despite being as affected in length as the *Ror2*$^{W749FLAG/W749FLAG}$ digits.

segmentation of the phalangeal rays. To investigate the potential mechanism, in situ hybridization with markers of limb patterning was performed.

Hoxd11-Hoxd13 are essential for normal patterning of the mouse autopod, and targeted disruption of any one of them causes autopod phenotypes reminiscent to *Ror2*$^{W749FLAG/W749FLAG}$ (Davis and Capecchi, 1994; Davis and Capecchi, 1996). However, *Hoxd11*, *Hoxd12*, and *Hoxd13* expression is not affected in *Ror2*$^{W749FLAG/W749FLAG}$ limbs at E12.5, a stage at which phalanges are being specified (see Fig. S1 in the supplementary material). Similarly, the expression patterns of *Shh* and *Fgf8* were not altered in mutant embryos during E11.5-E13.5 (see Fig. S2 in the supplementary material), indicating that the effect of ROR2 truncation on autopod bone length and patterning is independent of the SHH-HOXD signaling pathway and the SHH-FGF feedback loop.

Finally, the expression of *Gdf5*, an early marker of joint interzones, was examined. E12.5 *Ror2*$^{W749FLAG/W749FLAG}$ limbs showed the correct pattern of *Gdf5* expression expected at this stage; diffuse expression in the inter-digital mesenchyme and more intense expression in the outerzone of condensation and in the presumptive metacarpo-phalangeal joint interzones as the growth of the digital rays advances (Storm and Kingsley, 1996) (Fig. 8A,B). At E13.5, expression of *Gdf5* in *Ror2*$^{W749FLAG/W749FLAG}$ limbs was correctly restricted to the region of the presumptive digit joints but it showed a decreased intensity and domain in the presumptive proximal interphalangeal interzone (Fig. 8D, arrow). At later stages, expression was detected in the proximal interphalangeal interzone, whereas the region of the presumptive distal interzone failed to show *Gdf5* expression (Fig. 8E,F; see also Fig. S3 in the supplementary material). Thus, ROR2^{W749FLAG} seems to interfere with the specification of the distal digit interzone and the subsequent formation of the P2/P3 synovial joint.

DISCUSSION

Ror2$^{W749FLAG/W749FLAG}$ mice as a model of recessive Robinow syndrome

Mutations in *Ror2* are responsible for two classes of rare genetic disorders in humans, BDB and RRS, which display distinct modes of inheritance (autosomal dominant and recessive, respectively) and are associated with different sets of gene mutations. In this study, we generated mice bearing the W749X mutation in *Ror2*, which in humans results in a severe form of BDB. Our results show that *Ror2*^{W749FLAG} does not result in dominant brachydactyly in the mouse. Rather it causes abnormalities similar to those of *Ror2* knockout mice, without, however, causing the perinatal lethality observed in these lines. In this respect, it provides an animal model most closely resembling RRS.

In contrast to BDB, which only affects the digits, *Ror2*$^{W749FLAG/W749FLAG}$ mice exhibit abnormalities in the whole skeleton. Similar to RRS patients and *Ror2* knockout mice,

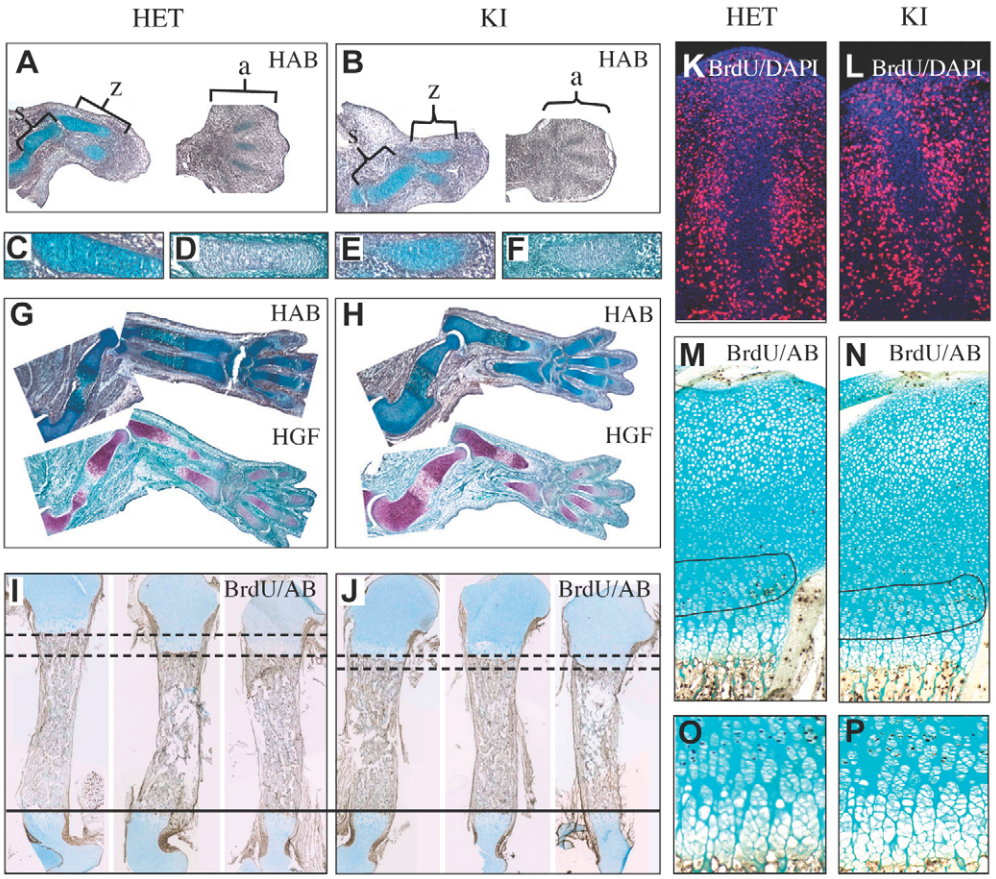

Fig. 7. Anlagen growth and chondrocyte proliferation are unaffected in *Ror2*$^{W749FLAG/W749FLAG}$ embryos. (**A**,**B**) Forelimb sections from *Ror2*$^{+/W749FLAG}$ (HET, A) and *Ror2*$^{W749FLAG/W749FLAG}$ (KI, B) E13.5 embryos stained with HAB reveal decreased cell numbers in the cartilagenous condensations of the mutant limbs. Stylopod (s), zeugopod (z) and autopod (a) are indicated. (**C-F**) High magnification of E13.5 ulna sections stained with HAB (C,E) or HGF (D,F), showing normal cell density and intensity of matrix staining. (**G**,**H**) Forelimb sections from *Ror2*$^{+/W749FLAG}$ (G) and *Ror2*$^{W749FLAG/W749FLAG}$ (H) E15.5 embryos stained with HAB and HGF. No overt histological alterations are observed in cell density or matrix staining, but the *Ror2*$^{W749FLAG/W749FLAG}$ bones are shorter, and have a smaller region of hypertrophy and primary spongiosa. (**I**,**J**) Sections of E18.5 humeri from three individual *Ror2*$^{+/W749FLAG}$ (I) and *Ror2*$^{W749FLAG/W749FLAG}$ (J) embryos stained with an anti-BrdU antibody and counterstained with AB. *Ror2*$^{W749FLAG/W749FLAG}$ humeri have a reduced length and shorter epiphyses (epiphysis range is indicated with horizontal lines). No difference was observed in the density or distribution of BrdU-positive cells. (**K-N**) BrdU incorporation analysis in E12.5 digital rays (K,L) and proliferative zone of postnatal P5 femurs (M,N, zone delineated) from *Ror2*$^{+/W749FLAG}$ (HET) and *Ror2*$^{W749FLAG/W749FLAG}$ (KI) littermate mice. (K,L) Proliferative rates were assayed in E12.5 rays by measuring the number of BrdU-positive nuclei (red) relative to the total number of nuclei (blue) in the condensation. No significant difference was observed between the genotypes (12.2±0.04% versus 12.5±0.05% in the controls, P=0.069). (M,N) BrdU incorporation analysis in postnatal P5 femurs showed no significant difference between genotypes (383±41.9 versus 373±60.5 cells/mm^2 in the controls, P=0.90). (**O**,**P**) High magnification of the growth plates from the sections shown in M and N, respectively, revealing a normal architecture of the columnar chondrocytes.

Ror2$^{W749FLAG/W749FLAG}$ mice show hemivertebrae, rib fusions, and shortening of the long bones. In the digits, a missing phalanx causes brachydactyly, a feature also described in the *Ror2*$^{TMlacZ/TMlacZ}$ mice (DeChiara et al., 2000) and found in some RRS families. Furthermore, about 5% of the animals present a duplicated digit I in the right hind limb, a phenotype also observed in 20% of the *Ror2*^{TMlacZ} mutants that may be related to the bifid thumbs shown by some RRS patients (Oldridge et al., 2000; Schwabe et al., 2004). The craniofacial defects, characterized by midfacial hypoplasia due to shortened nasal and jaw bones, resemble those of *Ror2* knockout mice, albeit manifested to a milder degree. Although hypertelorism, a feature of RRS patients and *Ror2*$^{-/-}$ mice (Schwabe et al., 2004), is not detected in *Ror2*$^{W749FLAG/W749FLAG}$, a wider intra-orbital space, and entropion with epiphora and dochitis are observed. It is possible that changes in the orbital bones of *Ror2*$^{W749FLAG/W749FLAG}$ mice affect the architecture of the naso-lacrimal ducts, resulting in obstruction and dochitis (Meyer, 1993), as is observed in brachycephalic canine and feline breeds. Overall, in mice, the mutation *Ror2*^{W749FLAG} does not phenocopy the human BDB phenotype associated with this mutation, resulting instead in a mouse model resembling RRS.

The different pattern of inheritance of the W749X mutation in humans compared with in mice may reflect differences in skeletal development between the two species (Wilkie, 2003), or may be attributed to genetic background effects on the expression of the mutation. Indeed, there are examples of distal phalanx brachydactyly in RRS patients (Patton and Afzal, 2002; Balci et al., 1993), and, conversely, of facial hypertelorism, hypoplastic alae nasi, and high nasal bridge and arched palate in some BDB cases (Hamamy et al., 2006). These observations suggest an overlap in the spectra of clinical features caused by BDB and RRS mutations.

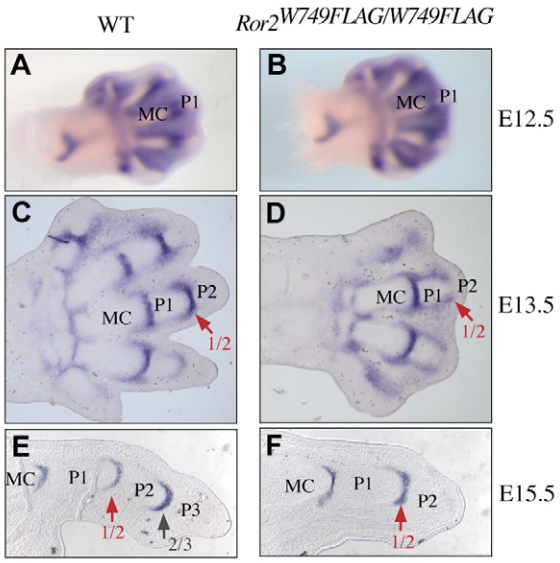

Fig. 8. Absence of *Gdf5* expression in the distal phalangeal interzone of *Ror2*$^{W749FLAG/W749FLAG}$ mutants. *Gdf5* expression was analyzed by in situ hybridization in limbs from wild-type (WT, A,C,E) and *Ror2*$^{W749FLAG/W749FLAG}$ (B,D,F) embryos. (**A**,**B**) Whole-mount in situ hybridization of forelimbs from E12.5 embryos, showing identical patterns of *Gdf5* expression in the mutant. (**C**,**D**) Sections of E13.5 forelimbs, revealing reduced expression of *Gdf5* in the proximal phalangeal interzone of *Ror2*$^{W749FLAG/W749FLAG}$ digits (D, 1/2). (**E**,**F**) Sections from E15.5 digits, showing normal *Gdf5* expression levels in the proximal phalangeal interzone of the *Ror2*$^{W749FLAG/W749FLAG}$ digit (F, 1/2), but absence of signal in the presumptive distal interzone (2/3). MC, metacarpal; P1, phalanx 1; P2, phalanx 2.

The skeletal hypoplasia observed in *Ror2*$^{W749FLAG/W749FLAG}$ mice can be traced back in development to the formation of chondrogenic condensations, which are all reduced in size in mutant embryos. Once formed, *Ror2*$^{W749FLAG/W749FLAG}$ condensations develop normally, except for a delay with respect to controls. However, this is not accompanied by changes in the number or density of BrdU-labeled cells in the cartilage (E12.5, E18.5) or in the growth plates (P5). This is in agreement with observations in *Ror2*$^{-/-}$ mice (Schwabe et al., 2004), or after the overexpression of dominant-negative forms of Ror2 in chicken (Stricker et al., 2006). Growth of the cartilaginous anlagen is a complex process that results from cellular recruitment from the mesenchyme underlying the perichondrium, as well as from chondrocyte proliferation in the hyaline cartilage and, especially, in the growth plates of the long bones, once they are formed (Dodds, 1930). We do not observe changes in chondrocyte proliferation in *Ror2*$^{W749FLAG/W749FLAG}$ mice; however, a reduction in the initial size of all of the chondrogenic condensations, a crucial parameter in determining the dimensions of the final skeletal development (Atchley and Hall, 1991), is observed. These results are consistent with an effect of *Ror2*^{W749FLAG} in the recruitment of mesenchymal cells into the chondrogenic condensation, rather than with an effect on elongation of the cartilage anlagen.

ROR2 cytoplasmic truncations cause missing phalanx and brachydactyly in the mouse

Ror2$^{W749FLAG/W749FLAG}$ mice show brachydactyly due to a missing phalanx in digits II to IV, a feature shared with *Ror2*$^{TMlacZ/TMlacZ}$ mice. Brachydactyly in BDB and RRS patients is thought to result from gain-of-function mutations of *ROR2*, as individuals carrying deletions encompassing the whole locus do not exhibit defects in the digits (Oldridge et al., 2000). Evidence in support of this interpretation is provided by *Ror2*$^{TMlacZ/TMlacZ}$ and *Ror2*-null mice; although both exhibit very similar defects in the skeleton, *Ror2*-null pups show a normal number of phalanges, whereas *Ror2*$^{TMlacZ/TMlacZ}$ mice fail to develop the distal interphalangeal (P2/P3) joint. Therefore, although ROR2 is dispensable for normal joint specification, cytoplasmic truncations of ROR2 disrupt the specification of the P2/P3 joint. The skeletal abnormalities of *Ror2*$^{W749FLAG/W749FLAG}$ or *Ror2*$^{TMlacZ/TMlacZ}$ mice may thus be interpreted as compound phenotypes, resulting from a combination of the loss of normal ROR2 function (skeletal syndrome observed in all *Ror2* mutants) and newly acquired ROR2 functions (interference with distal joint specification, observed in *Ror2*^{W749FLAG} and *Ror2*^{TMlacZ}, but not in mice lacking *Ror2*).

Most of the synovial joints in the limb, including those in the digits, form through segmentation of a single pre-existing cartilaginous condensation at the interzone (Archer et al., 2003). *Gdf5* expression is crucial for normal joint development and represents one of the earliest markers of interzone formation, preceding any morphological sign of specification (Storm and Kingsley, 1999). No *Gdf5* expression can be detected in *Ror2*^{W749FLAG} mutants at the site of the presumptive distal interzone, indicating that truncated ROR2 impairs distal joint specification at a very early stage, upstream of GDF5. Wnt is an upstream regulator of GDF5 in chondrocytes and is thought to be important for joint formation through the induction of GDF5 (Hartmann and Tabin, 2001; Guo et al., 2004; Tamamura et al., 2005). As ROR2 can interact with several Wnts (Billiard et al., 2005; Mikels and Nusse, 2006; Hamamy et al., 2006; Oishi et al., 2003), it is conceivable that ROR2 cytoplasmic truncations exert an inhibitory effect on Wnt signaling at the developing joint through non-productive interactions with Wnt ligands. Indeed, genetic and biochemical evidence in *C. elegans* shows that the extracellular domain of CAM-1 (the only *C. elegans* ROR homolog) is sufficient to antagonize multiple Wnts in a non-cell-autonomous manner, suggesting that CAM-1 buffers Wnt levels through sequestration (Green et al., 2007). The high degree of similarity shared by nematode and mammalian ROR proteins suggests a conserved ability of ROR receptors to modulate Wnt signaling in a cell-membrane-dependent, but kinase-independent, manner.

It has been proposed that during segmentation of the cartilaginous condensations, each new joint is formed at a distance from the previous one by spatial recovery from Noggin-inhibitory signals (Wnt, GDF5, BMPs) that emanate from the previous interzone (Guo et al., 2004). Under this model, the lack of the distal digital joint in *Ror2* mutants could be explained by the shorter length of the digital ray condensations, which would not provide enough distance at the distal end to allow concentrations of a joint-inducing activity to recover from the inhibitory field of the proximal joint. However, if this were the mechanism responsible for lack of the P2/P3 joint in the *Ror2*$^{W749FLAG/W749FLAG}$ digits, we would also expect *Ror2*$^{-/-}$ mice to lack the P2/P3 joint, as their developing digits are as short as those of *Ror2*$^{TMlacZ/TMlacZ}$ and *Ror2*$^{W749FLAG/W749FLAG}$ mice (Fig. 6H,I,T,U). Yet, *Ror2*$^{-/-}$ mice show normal specification of the digital joints. These observations support a direct role of ROR2 cytoplasmic truncations in blockage of formation of the P2/P3 joint.

Ror2$^{W749FLAG/W749FLAG}$ mice uncover effects of ROR2 on body composition and male fertility

Survival of the *Ror2*^{W749FLAG} homozygous mutant mice makes them useful for studying the role of ROR2 in adult bone. Based on studies using cell lines and mouse calvarial primary cultures, it has been

proposed that ROR2 promotes both osteoblast differentiation and the commitment of mesenchymal stem cells to the osteoblastic lineage (Liu et al., 2006). Although at 3 weeks of age *Ror2*$^{W749FLAG/W749FLAG}$ mice exhibit a reduction in trabecular bone volume, this phenotype is consistent with the delay in embryonic bone development and resolves later in life. Histomorphometric analysis of femoral bones shows that *Ror2*^{W749FLAG} has no major role in adult bone homeostasis.

The mutation, however, uncovers previously unrecognized effects of ROR2 in other organs. *Ror2*$^{W749FLAG/W749FLAG}$ mice display a lean phenotype with a normal metabolic rate, insulin tolerance, and adsorption and elimination of glucose. The reduced adiposity of *Ror2*^{W749FLAG} homozygous mice may result from developmental changes affecting the differentiation program of embryonic mesenchymal stem cells into fat and muscle lineages (Taylor and Jones, 1979). Consistent with this interpretation, ROR2 overexpression has been reported to affect the adipogenic differentiation of human mesenchymal stem cells (Liu et al., 2006).

Ror2$^{W749FLAG/W749FLAG}$ males are hypogonadic, as a result of focal degeneration of seminiferous tubules, have a reduced sperm count and show a markedly reduced fertility rate. In testes from 16-day-old mutant mice, all of the seminiferous tubules show a reduced diameter, contain a single layer of spermatogonia, and are devoid of spermatocytes. This suggests a role of ROR2 in the differentiation of germ cells during early puberty. The testicular and reproductive phenotype of *Ror2*$^{W749FLAG/W749FLAG}$ mice is very similar to that of *Bmp8*^{tm1blh} homozygous males, which exhibit infertility and dual defects in spermatogenesis: delay in the initiation of germ cell proliferation during early testicular development; and focal tubular degeneration in the mature testis (Zhao et al., 1996). It will be interesting to investigate whether ROR2 and BMP8B act in the same pathway during spermatogenesis.

We thank all at Regeneron Pharmaceuticals for their assistance, especially the VelociGene and RAF cores for targeting vectors, blastocyst injections, and mouse breeding and genotyping. We also thank S. Statton for graphic support, S. Croll for statistical analysis, T. Rakowski-Anderson for the diagnosis of entropion, and CRL for histopathology and IVF services. In part supported by grants DK 42424 and DK 45227 from the National Institutes of Diabetes, Digestive and Kidney Disease (E.C.), and grant SFB577 from the Deutsche Forschungsgemeinschaft (S.S. and S.M.).

Supplementary material

Supplementary material for this article is available at http://dev.biologists.org/cgi/content/full/135/9/1713/DC1

References

Afzal, A. R. and Jeffery, S. (2003). One gene, two phenotypes: ROR2 mutations in autosomal recessive Robinow syndrome and autosomal dominant brachydactyly type B. *Hum. Mutat.* **22**, 1-11.

Albrecht, A. N., Schwabe, G. C., Stricker, S., Boddrich, A., Wanker, E. E. and Mundlos, S. (2002). The synpolydactyly homolog (spdh) mutation in the mouse – a defect in patterning and growth of limb cartilage elements. *Mech. Dev.* **112**, 53-67.

Archer, C. W., Dowthwaite, G. P. and Francis-West, P. (2003). Development of synovial joints. *Birth Defects Res. C Embryo Today* **69**, 144-155.

Atchley, W. R. and Hall, B. K. (1991). A model for development and evolution of complex morphological structures. *Biol. Rev. Camb. Philos. Soc.* **66**, 101-157.

Balci, S., Ercal, M. D., Say, B. and Atasu, M. (1993). Robinow syndrome: with special emphasis on dermatoglyphics and hand malformations (split hand). *Clin. Dysmorphol.* **2**, 199-207.

Billiard, J., Way, D. S., Seestaller-Wehr, L. M., Moran, R. A., Mangine, A. and Bodine, P. V. (2005). The orphan receptor tyrosine kinase Ror2 modulates canonical Wnt signaling in osteoblastic cells. *Mol. Endocrinol.* **19**, 90-101.

Davis, A. P. and Capecchi, M. R. (1994). Axial homeosis and appendicular skeleton defects in mice with a targeted disruption of hoxd-11. *Development* **120**, 2187-2198.

Davis, A. P. and Capecchi, M. R. (1996). A mutational analysis of the 5′ HoxD genes: dissection of genetic interactions during limb development in the mouse. *Development* **122**, 1175-1185.

DeChiara, T. M., Kimble, R. B., Poueymirou, W. T., Rojas, J., Masiakowski, P., Valenzuela, D. M. and Yancopoulos, G. D. (2000). Ror2, encoding a receptor-like tyrosine kinase, is required for cartilage and growth plate development. *Nat. Genet.* **24**, 271-274.

Dodds, G. S. (1930). Row formation and other types of arrangement of cartilage ceils in. endochondral ossification. *Anat. Rec.* **46**, 385-399.

Forrester, W. C. (2002). The Ror receptor tyrosine kinase family. *Cell. Mol. Life Sci.* **59**, 83-96.

Gazzerro, E., Pereira, R. C., Jorgetti, V., Olson, S., Economides, A. N. and Canalis, E. (2005). Skeletal overexpression of gremlin impairs bone formation and causes osteopenia. *Endocrinology* **146**, 655-665.

Green, J. L., Inoue, T. and Sternberg, P. W. (2007). The C. elegans ROR receptor tyrosine kinase, CAM-1, non-autonomously inhibits the Wnt pathway. *Development* **134**, 4053-4062.

Guo, X., Day, T. F., Jiang, X., Garrett-Beal, L., Topol, L. and Yang, Y. (2004). Wnt/beta-catenin signaling is sufficient and necessary for synovial joint formation. *Genes Dev.* **18**, 2404-2417.

Hamamy, H., Saleh, N., Oldridge, M., Al-Hadidy, A. and Ajlouni, K. (2006). Brachydactyly type B1: report of a family with de novo ROR2 mutation. *Clin. Genet.* **70**, 538-540.

Hartmann, C. and Tabin, C. J. (2001). Wnt-14 plays a pivotal role in inducing synovial joint formation in the developing appendicular skeleton. *Cell* **104**, 341-351.

Healy, C., Uwanogho, D. and Sharpe, P. T. (1996). Expression of the chicken Sox9 gene marks the onset of cartilage differentiation. *Ann. New York Acad. Sci.* **785**, 261-262.

Hikasa, H., Shibata, M., Hiratani, I. and Taira, M. (2002). The Xenopus receptor tyrosine kinase Xror2 modulates morphogenetic movements of the axial mesoderm and neuroectoderm via Wnt signaling. *Development* **129**, 5227-5239.

Ippolito, E., Pedrini, V. A. and Pedrini-Mille, A. (1983). Histochemical properties of cartilage proteoglycans. *J. Histochem. Cytochem.* **31**, 53-61.

Jegalian, B. G. and De Robertis, E. M. (1992). Homeotic transformations in the mouse induced by overexpression of a human Hox3.3 transgene. *Cell* **71**, 901-910.

Liu, Y., Bhat, R. A., Seestaller-Wehr, L. M., Fukayama, S., Mangine, A., Moran, R. A., Komm, B. S., Bodine, P. V. and Billiard, J. (2006). The orphan receptor tyrosine kinase Ror2 promotes osteoblast differentiation and enhances ex vivo bone formation. *Mol. Endocrinol.* **21**, 376-387.

Lufkin, T., Mark, M., Hart, C. P., Dolle, P., LeMeur, M. and Chambon, P. (1992). Homeotic transformation of the occipital bones of the skull by ectopic expression of a homeobox gene. *Nature* **359**, 835-841.

Marie, I., Durbin, J. E. and Levy, D. E. (1998). Differential viral induction of distinct interferon-alpha genes by positive feedback through interferon regulatory factor-7. *EMBO J.* **17**, 6660-6669.

Masiakowski, P. and Yancopoulos, G. D. (1998). The Wnt receptor CRD domain is also found in MuSK and related orphan receptor tyrosine kinases. *Curr. Biol.* **8**, R407.

Meyer, D. R. (1993). Lacrimal disease and surgery. *Curr. Opin. Ophthalmol.* **4**, 86-94.

Mikels, A. J. and Nusse, R. (2006). Purified Wnt5a protein activates or inhibits beta-catenin-TCF signaling depending on receptor context. *PLoS Biol.* **4**, e115.

Oishi, I., Suzuki, H., Onishi, N., Takada, R., Kani, S., Ohkawara, B., Koshida, I., Suzuki, K., Yamada, G., Schwabe, G. C. et al. (2003). The receptor tyrosine kinase Ror2 is involved in non-canonical Wnt5a/JNK signalling pathway. *Genes Cells* **8**, 645-654.

Oldridge, M., Temple, I. K., Santos, H. G., Gibbons, R. J., Mustafa, Z., Chapman, K. E., Loughlin, J. and Wilkie, A. O. (1999). Brachydactyly type B: linkage to chromosome 9q22 and evidence for genetic heterogeneity. *Am. J. Hum. Genet.* **64**, 578-585.

Oldridge, M., Fortuna, A. M., Maringa, M., Propping, P., Mansour, S., Pollitt, C., DeChiara, T. M., Kimble, R. B., Valenzuela, D. M., Yancopoulos, G. D. et al. (2000). Dominant mutations in ROR2, encoding an orphan receptor tyrosine kinase, cause brachydactyly type B. *Nat. Genet.* **24**, 275-278.

Parfitt, A. M., Drezner, M. K., Glorieux, F. H., Kanis, J. A., Malluche, H., Meunier, P. J., Ott, S. M. and Recker, R. R. (1987). Bone histomorphometry: standardization of nomenclature, symbols, and units. Report of the ASBMR Histomorphometry Nomenclature Committee. *J. Bone Miner. Res.* **2**, 595-610.

Patton, M. A. and Afzal, A. R. (2002). Robinow syndrome. *J. Med. Genet.* **39**, 305-310.

Saldanha, J., Singh, J. and Mahadevan, D. (1998). Identification of a Frizzled-like cysteine rich domain in the extracellular region of developmental receptor tyrosine kinases. *Protein Sci.* **7**, 1632-1635.

Schwabe, G. C., Tinschert, S., Buschow, C., Meinecke, P., Wolff, G., Gillessen-Kaesbach, G., Oldridge, M., Wilkie, A. O., Komec, R. and Mundlos, S. (2000). Distinct mutations in the receptor tyrosine kinase gene ROR2 cause brachydactyly type B. *Am. J. Hum. Genet.* **67**, 822-831.

Schwabe, G. C., Trepczik, B., Suring, K., Brieske, N., Tucker, A. S., Sharpe, P. T., Minami, Y. and Mundlos, S. (2004). Ror2 knockout mouse as a model for

the developmental pathology of autosomal recessive Robinow syndrome. *Dev. Dyn.* **229**, 400-410.
Storm, E. E. and Kingsley, D. M. (1996). Joint patterning defects caused by single and double mutations in members of the bone morphogenetic protein (BMP) family. *Development* **122**, 3969-3979.
Storm, E. E. and Kingsley, D. M. (1999). GDF5 coordinates bone and joint formation during digit development. *Dev. Biol.* **209**, 11-27.
Stricker, S., Fundele, R., Vortkamp, A. and Mundlos, S. (2002). Role of Runx genes in chondrocyte differentiation. *Dev. Biol.* **245**, 95-108.
Stricker, S., Verhey van Wijk, N., Witte, F., Brieske, N., Seidel, K. and Mundlos, S. (2006). Cloning and expression pattern of chicken Ror2 and functional characterization of truncating mutations in Brachydactyly type B and Robinow syndrome. *Dev. Dyn.* **235**, 3456-3465.
Takeuchi, S., Takeda, K., Oishi, I., Nomi, M., Ikeya, M., Itoh, K., Tamura, S., Ueda, T., Hatta, T., Otani, H. et al. (2000). Mouse Ror2 receptor tyrosine kinase is required for the heart development and limb formation. *Genes Cells* **5**, 71-78.
Tamamura, Y., Otani, T., Kanatani, N., Koyama, E., Kitagaki, J., Komori, T., Yamada, Y., Costantini, F., Wakisaka, S., Pacifici, M. et al. (2005). Developmental regulation of Wnt/beta-catenin signals is required for growth plate assembly, cartilage integrity, and endochondral ossification. *J. Biol. Chem.* **280**, 19185-19195.
Taylor, S. M. and Jones, P. A. (1979). Multiple new phenotypes induced in 10T1/2 and 3T3 cells treated with 5-azacytidine. *Cell* **17**, 771-779.
Tribioli, C. and Lufkin, T. (1999). The murine Bapx1 homeobox gene plays a critical role in embryonic development of the axial skeleton and spleen. *Development* **126**, 5699-5711.
Valenzuela, D. M., Murphy, A. J., Frendewey, D., Gale, N. W., Economides, A. N., Auerbach, W., Poueymirou, W. T., Adams, N. C., Rojas, J., Yasenchak, J. et al. (2003). High-throughput engineering of the mouse genome coupled with high-resolution expression analysis. *Nat. Biotechnol.* **21**, 652-659.
Wilkie, A. O. (2003). Why study human limb malformations? *J. Anat.* **202**, 27-35.
Zhao, G. Q., Deng, K., Labosky, P. A., Liaw, L. and Hogan, B. L. (1996). The gene encoding bone morphogenetic protein 8B is required for the initiation and maintenance of spermatogenesis in the mouse. *Genes Dev.* **10**, 1657-1669.